

Time-correlated single-photon counting fluorescence lifetime confocal imaging of decayed and sound dental structures with a white-light supercontinuum source

G. McCONNELL*, J. M. GIRKIN†, S. M. AMEER-BEG‡§, P. R. BARBER‡, B. VOJNOVIC‡, T. NG§, A. BANERJEE¶, T. F. WATSON¶ & R. J. COOK¶

*Centre for Biophotonics, Strathclyde Institute of Pharmacy and Biomedical Sciences, University of Strathclyde, 27 Taylor Street, Glasgow, G4 0NR, UK

†Institute of Photonics, University of Strathclyde, 106 Rottenrow, Glasgow, G4 0NW, UK

‡Advanced Technology Development Group, Gray Cancer Research Institute, PO Box 100, Mount Vernon Hospital, Northwood, Middlesex, HA6 2JR, UK

§Richard Dimbleby Department Of Cancer Research, Division of Cancer Studies & Randall Division of Cell and Molecular Biophysics, King's College London, Floor 3, New Hunts House, Guy's Medical School Campus, London, SE1 1UL, UK

¶Department of Microscopy & Imaging, King's College London Dental Institute, Floor 17 Guy's Tower, Guy's Hospital, London, SE1 9RT, UK

Key words. PACS: 42.62.Be Biological and medical applications, 42.65.-k nonlinear optics, 87.64.Ni optical absorption, magnetic circular dichroism, fluorescence spectroscopy.

Summary

We report the demonstration of time-correlated single-photon counting (TCSPC) fluorescence lifetime imaging (FLIM) to *ex vivo* decayed and healthy dental tooth structures, using a white-light supercontinuum excitation source. By using a 100 fs-pulsed Ti:Sapphire laser with a low-frequency chirp to pump a 30-cm long section of photonic crystal fibre, a ps-pulsed white-light supercontinuum was created. Optical bandpass interference filters were then applied to this broad-bandwidth source to select the 488-nm excitation wavelength required to perform TCSPC FLIM of dental structures. Decayed dentine showed significantly shorter lifetimes, discriminating it from healthy tissue and hard, stained and thus affected but non-infected material. The white-light generation source provides a flexible method of producing variable-bandwidth visible and ps-pulsed light for TCSPC FLIM. The results from the dental tissue indicate a potential method of discriminating diseased tissue from sound, but stained tissue, which could be of crucial importance in limiting tissue resection during preparation for clinical restorations.

Introduction

Fluorescence lifetime imaging microscopy (FLIM) is a burgeoning technique that exploits intensity-independent contrast imaging based upon the characteristic fluorescence lifetime (τ) of any given fluorophore and potential changes induced by an inhomogeneous environment (Marriott *et al.*, 1991). Images obtained via FLIM therefore offer the opportunity to explore cellular and tissue structures at the molecular level (Gadella & Jovin, 1995; Ng *et al.*, 2001; Anilkumar *et al.*, 2003). Local conditions such as pH, oxygen levels and hydration as well as chemical composition are well recognized as influencers of fluorescence lifetime (Koenig & Schneckenburger, 1994; Koenig *et al.*, 1998; Kwak *et al.*, 2001; Gannot *et al.*, 2004). Thus in natural biological tissue, local conditions and disease can cause significant changes to the lifetime of the fluorophore, providing additional information on the status of the material.

Koenig & Schneckenburger (1994) note the first use of Wood's ultraviolet lamp by Bommer to demonstrate dental plaque via red/orange auto-fluorescence as early as 1927. It is widely accepted that bacterially infected calculus and decayed dentine exhibit greater intensity auto-fluorescence emission ~650–700 nm than sound enamel, dentine and

cementum using blue excitation wavelengths (Koenig *et al.*, 1993; Taubinsky *et al.*, 2000; Kurihara *et al.*, 2004; Buchalla, 2005).

Decayed dentine auto-fluorescence occurs at a multitude of excitation and emission wavelengths (Banerjee & Boyde, 1998; Kwak *et al.*, 2001). This is most probably attributed to an aggregate of multiple potential fluorophores including collagens and elastins, individual amino acids (e.g. tryptophan and tyrosine), porphyrin molecules including protoporphyrin IX, coenzymes such as NAD(P)H and flavin molecules, plasma proteins such as albumin (via tryptophan at residue 214), alpha-2HS-glycoprotein and hydroxypyridinium (Foreman, 1980; Alfano & Yao, 1981; Odetti *et al.*, 1992; Schneckenburger & Koenig, 1992; Schomacker *et al.*, 1992; Koenig *et al.*, 1993; Kwak *et al.*, 2001; Stortelder *et al.*, 2004). An additional and often overlooked incidental dentine fluorophore is the tetracycline antibiotic compound group, incrementally bound to the organic matrix, with secondary calcium binding that is present if administered during odontogenesis (i.e. in early childhood and adolescence) (Foreman, 1980).

Bulk sound dental material fluorescence is capitalized on in quantitative laser fluorescence (QLF) – in which, early uninfected and noncavitated enamel decay is detected as a quantifiable fluorescence radiance change – macroscopic dark red/brown regions set against a background gross green auto-fluorescence in response to blue wavelength excitation (van der Veen *et al.*, 2000; Mujat *et al.*, 2003, 2004). Some suggest the phenomena is explained by perturbations of bulk dentine fluorescence emissions transmitted through uninfected, noncavitated but optically active subsurface demineralized enamel prism lesion sites producing an apparent red shift effect (van der Veen *et al.*, 2000; Mujat *et al.*, 2003, 2004). Others propose additional bacterially sourced porphyrins as the cause (Koenig *et al.*, 1998; Taubinsky *et al.*, 2000; Buchalla, 2005), acquired from the overlying biofilm; later brown spot lesions demonstrating more intense red shift than early white spot lesions (Buchalla, 2005). The commercial infrared illumination Diagnodent system employs this principle (Haak & Wicht, 2004; Mendes *et al.*, 2004), but may often be defeated by other pigments, stains, plaque and reflections acquired by the host. Any such fluorophore would have to permeate the minimally porous lesion surface apatite layers; acid-eluted mineral being trapped and re-precipitated within the supersaturated zone beneath the overlying acidogenic biofilm in such early noncavitated lesions.

The bacterially derived acid attack in dental caries naturally progresses to outer surface cavitation by undermining at the enamel dentine junction. Perforation permits the first bacterial ingress, allowing colonization of internal dental tissues and subsequent breakdown of deeper structures by both continued acid demineralization and nonmineralized dentine matrix proteolysis.

Distinct from the protoporphyrin and other signatures noted above, a characteristic but uncharacterized yellow-green visible fluorescence signature (Schneckenburger & Koenig, 1992; Ng *et al.*, 2001) is also detectable in decayed dentine. The signature emission is localized to and follows the path of decayed dentine tubules, is excited by 488-nm wavelengths and is discriminated via 515 nm and abolished by >590-nm long pass filters (Banerjee, 1998; Banerjee & Boyde, 1998; Banerjee *et al.*, 1999, 2003, 2004). Confocal optical section imaging is necessary to discriminate the greater intensity decay emission from the otherwise overwhelming background bulk sound dentine fluorescence excited by the same 488-nm source (Banerjee, 1998; Banerjee & Boyde, 1998; Banerjee *et al.*, 1999, 2003, 2004).

At the infected decayed dentine stage, the lesions are easy to clinically detect and normally require operative intervention through the use of a dental bur to remove the infected material prior to restoration placement. The aim of the dental practitioner at this stage is to remove the minimum amount of tooth structure, thus ensuring its long-term survival. However, the desire to remove infected material can not be guided by colour as the remaining dentine is frequently stained due to a variety of causes. As hardness may be difficult to discern via dental cutting instruments, sound tissue may be removed inadvertently during cavity preparation due to poor discrimination of the infected/affected interface.

Due to the localized change in conditions and chemistries at such interfaces, fluorescence lifetimes could be expected to vary across the dentine lesion. FLIM may thus provide a method of discriminating between healthy and infected tissue, even when uninfected healthy tissue is stained, as is commonplace at the margins of decayed dentine lesions. Dental samples therefore offer interesting and highly complex real biological samples with which to investigate novel methods of lifetime imaging (Koenig *et al.*, 1998; Vroom *et al.*, 1999; de Grauw & Gerritsen, 2001; Webb *et al.*, 2002).

Time-correlated single-photon counting (TCSPC) involves the detection of single photons emitted by a fluorescent medium. These fluorescence photons are collected using a fast detector and electronics (O'Connor & Phillips, 1984), with count rates of up to 10^6 photons per second being possible using contemporary lifetime imaging modules. In a conventional system the fluorescence photon initiates a clock in the electronics, which is then stopped when the reference laser pulse is detected (reverse start stop TCSPC). By repeatedly making such measurements, the statistical profile of the time emission can be recorded. TCSPC can then be correlated with the fluorescence intensity image to provide lifetime and structural information (Becker *et al.*, 2001, 2004; Lamb *et al.*, 2005). To undertake TCSPC FLIM, one requires a high repetition rate pulsed excitation source whose excitation wavelength should be well-matched to the absorption wavelength(s) of the sample. Currently, the preferred options are either pulsed laser diodes for

single-photon excitation (Elson *et al.*, 2002) or via multiphoton excitation (Schonle *et al.*, 2000) although one previous report has made of the use of a white-light supercontinuum (WLS) source (Marriott *et al.*, 1991). In the single-photon excitation case, only a very limited number of discrete, fixed wavelengths are available. Although multiphoton excitation inherently provides optical sectioning capability, the lower excitation efficiency, limited tuning range (particularly the $\lambda = 1000\text{--}1200$ nm range) and simultaneous excitation of multiple fluorescent molecules are its limitations. Optical parametric oscillators have been used to perform both single- and multiphoton excited TCSPC FLIM; however, these sources are expensive, and are complex and difficult to operate (Maus *et al.*, 2001). We report a simple photon-efficient approach to overcome these technology limitations using photonic crystal fibre (PCF) technology to generate a WLS source from a pre-existing fs-pulsed Ti:Sapphire laser to perform TCSPC FLIM of dental samples. The very high peak powers present within the mode-locked pulses initiate a series of nonlinear processes within the fibre leading to a white-light output (Fedotov *et al.*, 2000). Several methods can then be used to select the required wavelength from the resulting white-light source to provide the optimal range of excitation wavelengths for the given specimen including the use of inexpensive optical bandpass interference filters. The adopted approach enabled both single-photon and multiphoton TCSPC FLIM to be undertaken using the same extant Ti:Sapphire platform source, avoiding the need for additional sources. The wide range of accessible wavelengths broadens the choice of fluorescent molecules that can be investigated using this powerful technique.

This report covers two advances, the first is a demonstration of the potential for use of PCF-based multi-wavelength sources for TCSPC FLIM of naturally occurring biological fluorescence and the second is the use of FLIM to non-invasively examine the extent of bacterially infected advanced dental caries with a long-term potential goal of developing technologies to guide and limit operative decayed dental tissues resection.

Experimental details

Optical configuration

The full experimental system is shown in Fig. 1. A 6W diode pumped, frequency doubled Nd:Vanadate laser (Verdi, Coherent, Inc., Santa Clara, CA, USA) was used to pump a fs-pulsed mode-locked Ti:Sapphire laser (Mira, Coherent, Inc.) wavelength-tunable from 720 nm to 930 nm. For this study, the laser was tuned to provide radiation at around 815 nm with a full-width half-maximum spectral bandwidth ($\Delta\lambda$) of 6 nm, measured using a simple CCD-based spectrometer (Ocean Optics bV, Duiven, Netherlands). The laser emitted an average output power of 600 mW at this wavelength, with a pulse repetition frequency of 76 MHz. The output was initially directed through a 4%

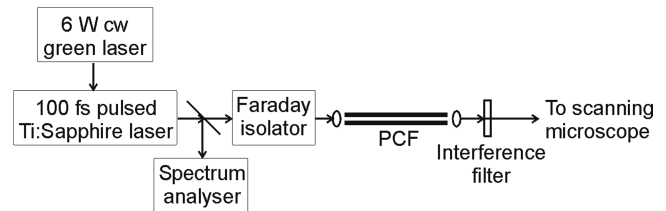


Fig. 1. Experimental set-up. The infrared ($\lambda = 812$ nm) output of an optically pumped fs-pulsed Ti:Sapphire laser was sent through a Faraday Isolator (E.I.) and coupled into a 30-cm section of anomalously dispersive photonic crystal fibre (PCF). The resultant white-light supercontinuum was filtered through a high-quality optical interference filter to spectrally filter the source prior to entering the scanning microscope's TCSPC system.

reflecting beam splitter with the pick-off light being sent into the spectrometer to monitor the laser performance. The remaining light was used as the platform source to create the WLS from the existing laboratory laser. Before entering the fibre aligning optics the light was passed through a Faraday isolator designed for operation at $\lambda = 820$ nm, which provided 30 dB of isolation. This was necessary to avoid feedback effects from the following optical elements that otherwise disrupted the pulse train from the Ti:Sapphire oscillator. The average power level of light leaving the Faraday isolator was measured to be 490 mW. This radiation was then focussed into the PCF using an aspheric lens with a focal length of $f = +3.1$ mm and a numerical aperture of 0.25. The average power following this lens was measured to be 465 mW, which then entered the PCF fibre.

The 30-cm long highly nonlinear PCF used to generate the WLS possessed a $1.5\text{-}\mu\text{m}$ core size with a pitch of $2.0 \pm 0.1 \mu\text{m}$ (NL-15-670, Crystal fibre, Birkerød, Denmark). This arrangement gave rise to a $\lambda = 670 \pm 0.5$ nm zero dispersion wavelength. When pumped with the Ti:Sapphire source at $\lambda = 812$ nm, the fibre operated in the anomalously dispersive regime and hence facilitated the creation of a WLS source in a simple manner. The WLS was collimated using a second aspheric lens with a focal length of $f = 8$ mm, NA 0.25 (Thorlabs, Inc., Newton, NJ, USA). The WLS was then propagated through an optical bandpass filter with a peak transmission wavelength of $\lambda = 480$ nm and a full-width at half-maximum transmission of $\Delta\lambda = 20$ nm. The spectrum of this $\lambda = 460\text{--}500$ nm source was captured using an optical spectrometer with $\lambda = 1$ -nm resolution (Ocean Optics). The filter selection was based upon previous work as it was known that 488-nm light was suitable for exciting the as yet unidentified fluorescent compound(s) of interest, exciting fluorescence in the visible yellow-green spectrum (Banerjee, 1998; Banerjee & Boyde, 1998; Banerjee *et al.*, 1999, 2003, 2004) and also that applying light beyond the FWHM of the absorption spectrum does not improve the FLIM image quality (Ameer-Beg *et al.*, 2002, 2003). The pulse duration of this visible radiation was estimated to be of the order of 10 ps. The resulting beam was around 20 mm in diameter

and was directed into a home built scanning system similar to that reported by Carlsson & Liljeborg (Carlsson & Liljeborg, 1989). This beam diameter overfilled the back aperture of the objective lenses used (18 mm) in order to ensure that the final illumination spot in the sample was as uniform in intensity as possible. A $\lambda = 510$ -nm dichroic optic placed just before the back aperture of the objective lens allowed direction of the excitation radiation towards the sample and reflection of the fluorescence signal towards the detector.

Detection of the emitted (fluorescence) photons was afforded by the use of fast single-photon response (Hamamatsu 7400, Hamamatsu Ltd., Hamamatsu, Japan) non-descanned detectors, developed in-house, situated in the re-imaged objective pupil plane. Fluorescence lifetime imaging capability was provided by time-correlated single-photon counting electronics (Becker & Hickl, SPC 830, Berlin, Germany). A $10\times$ objective was used throughout (Nikon, CFI60 SFluor N.A. 0.3, 16-mm working distance) and data were collected through a dichroic bandpass filter centred at $\lambda = 560 \pm 25$ nm (Chroma, Inc., Rockingham, VT, USA). Excitation power was adjusted using a neutral density filter to give average photon counting rates of the order 10^4 – 10^5 photons s^{-1} (0.0001–0.001 photon counts per excitation event) to avoid pulse pile up. Acquisition times of the order of 300 s at low excitation power were used to achieve sufficient photon statistics for fitting, while avoiding either pulse pile-up or observable photo-bleaching. The imaging system was controlled, and the data later analyzed, with custom software written in CVI LabWindows (Barber *et al.*, 2005). Each FLIM image comprised 256×256 pixels, with sub-ns temporal resolution being measured for the FLIM images whereas sub- μm resolution was observed within the matched $630 \mu\text{m} \times 630 \mu\text{m}$ high-contrast auto-fluorescence images taken using the PCF source and, for comparison, from the microscope's conventional mercury-arc-derived 488-nm illumination source.

Dental sample preparation

Three freshly extracted and grossly decayed human tooth specimens (Guy's & St Thomas' Trust ethical committee approval 04/Q0704/57) were cleaned to remove all soft tissue and then longitudinally sectioned through clinically obvious carious lesions, using a slow-speed diamond saw, running under water (Labcut 1010 saw & XL-1205 blade, Agar Scientific, Essex, UK). To avoid dehydration confounding the auto-fluorescence spectra, each sample was maintained in aqueous storage before preparation and imaging. No additional sectioned surface polishing or preparation was undertaken to avoid surface contamination. Prior to examination, a grid of light score marks was applied to the imaged surfaces using a sterile No. 11 scalpel blade to allow co-localization of auto-fluorescence images and FLIM maps back to the original sample surfaces. The sectioned surfaces of the sample were then imaged digitally at the macroscopic

level using a Nikon Coolpix 5000 camera in order to record the gross morphological structures within each specimen. Sites of interest ranged from sound unaffected dentine, to grossly softened destroyed dentine structure, the enamel-dentine junction and dentine/cementum root surfaces. The light score marks were used during the image analysis to enable co-localization of the conventional, fluorescence and FLIM images. The samples were mounted sectioned surface down on thin glass cover slips with an intervening aqueous film maintaining hydration during examination on the inverted microscope.

Results

The unfiltered PCF excitation spectrum derived from the existing Ti:Sapphire source used during the FLIM imaging is shown in Fig. 2. The spectrum shows some intensity fluctuations on the spectral structure but the intensity fluctuations were found to be significantly less than $\pm 0.25\%$ (rms). Repeated sampling of lifetime data throughout the experiments established a standard deviation of lifetime figure to be for the system, reliably at a level of ± 0.08 ns throughout.

Auto-fluorescence images taken using both the spectrally filtered PCF source and the mercury arc lamp were easily co-localized to sectioned decayed dentine samples using anatomical landmarks and score marks placed on the imaged surfaces (Fig. 3) to show the relative positions within the gross decay lesion of a bisected third permanent molar with gross occlusal decay (Fig. 3, panel 1 A).

Fluorescence intensity and cross-sectional TCSPC FLIM images of two sampled sites are presented in Fig. 3, panels 2 (I–IV) and 3 (I–IV), respectively. Site 3B and panel 2 were located at the margin of gross decay, straddling the interface of clinically soft and hard dentine and therefore includes the plane where a dental surgeon would be expected to suspend decay removal. The $1\text{-}\mu\text{m}$ diameter dentine tubule pattern was visualized

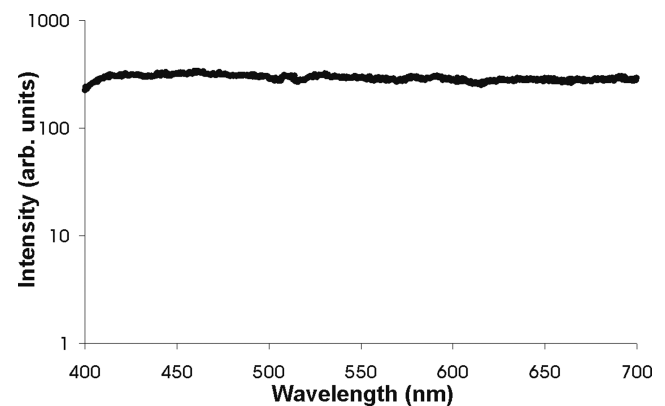


Fig. 2. Typical unfiltered white-light supercontinuum transmitted through the PCF, plotted on a linear scale. This corresponds to an average power of approximately 50 mW emitted through the PCF.

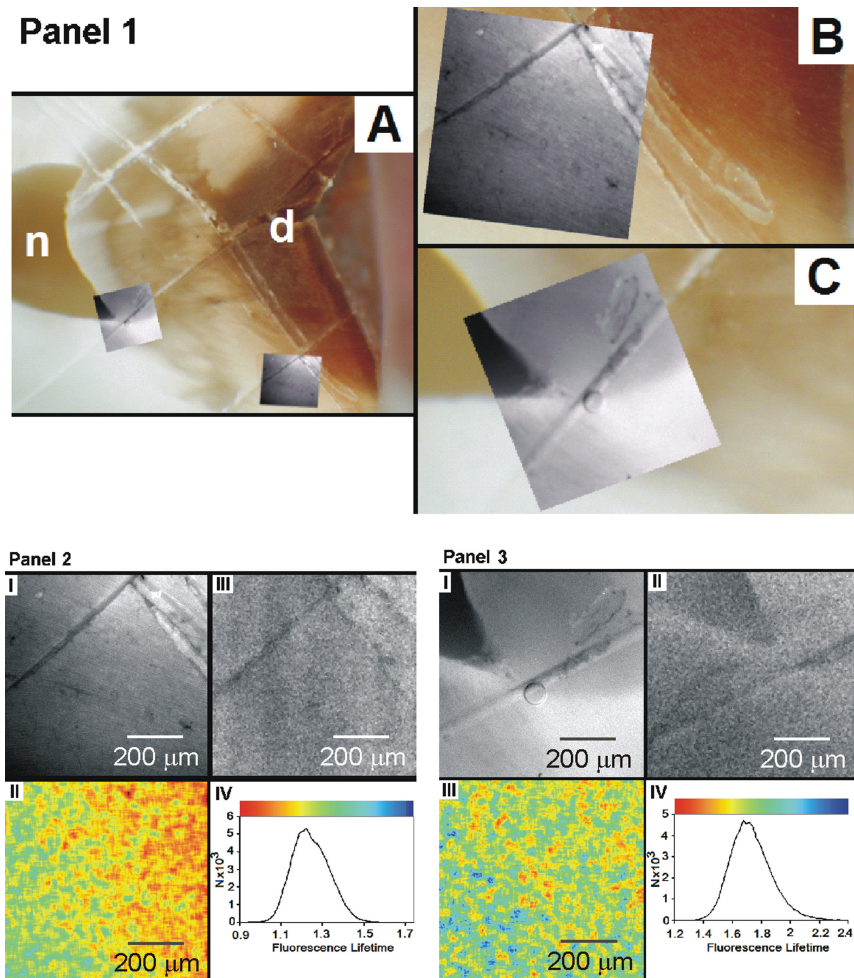


Fig. 3. Gross occlusal dentine decay (d) seen in a bisected human third permanent molar. Panel 1A shows the gross morphological appearance of the sectioned lesion sample (fieldwidth 5 mm), with conventional wide-field fluorescence images using incoherent mercury arc sourced 488-nm excitation auto-fluorescence images (B, C) co-localised via surface score marks and anatomical landmarks including the 1- μm diameter dentine tubule pattern, and the dental nerve (n) space. Panel 2 corresponds to the detailed imaging from the decayed margin at site B and panel 3 corresponds to stained but hard, deep dentine at site C. In panels 2 and 3 the image field widths are all 630 μm and in both panels image I is a conventional incoherent mercury arc 488-nm excitation auto-fluorescence image, II is the corresponding PCF laser source image and III shows the corresponding lifetime map, plotted as a lifetime histogram of number of photon counts (N) against lifetime in nanoseconds. At the interface of clinically hard stained and soft decayed dentine (d), signature auto-fluorescence intensity is seen to rise into the decay zone (panel 2 top right of images) as expected. FLIM mapping shows a significant lifetime variation across the interface (panel 2 – III). Panel 3 was chosen to reflect a clinically hard, discoloured but not directly involved region of the same dentine lesion located around the coronal tip or cornua of a pulp horn – the dental nerve (n). Data comparison shows a more uniform FLIM mapping in panel 3 and the FLIM histogram shows an approximate 40% increase in lifetime value with the distribution doubling from 0.45 to 0.8 ns wide, respectively, compared with the site B (panel 2) data.

as expected for the anatomical site, and auto-fluorescence signature intensity rose as expected within the decay zone. FLIM mapping across the interface (Fig. 3, panel 2 (III)) showed a significant variation in lifetime across the decay to sound tooth interface, the data range being shown in image IV.

By comparison, Fig. 3, panels 1C and 3 represent a far deeper point located in the same lesion but in clinically hard, non-infected dentine (i.e. affected by the decay process) and shows a more uniform FLIM map panel 3 (III), but the histogram

scale panel 3 (IV) is shifted to the right, the FLIM peaks having shifted from ~ 1.25 to ~ 1.75 ns (a 40% increase) with the lifetime histogram distribution doubling from 0.45 to 0.8 ns, respectively (cf. Fig. 4). Thus, both fluorescence lifetime and range of spread rises as decay gives way to affected (discoloured) but not directly involved dentine. PCF illuminated image quality was adversely affected by some prompt signal re-entry and scatter from tissue bulk beyond the optimal plane of focus. Further focus was less simple to achieve with the PCF illumination source functioning.

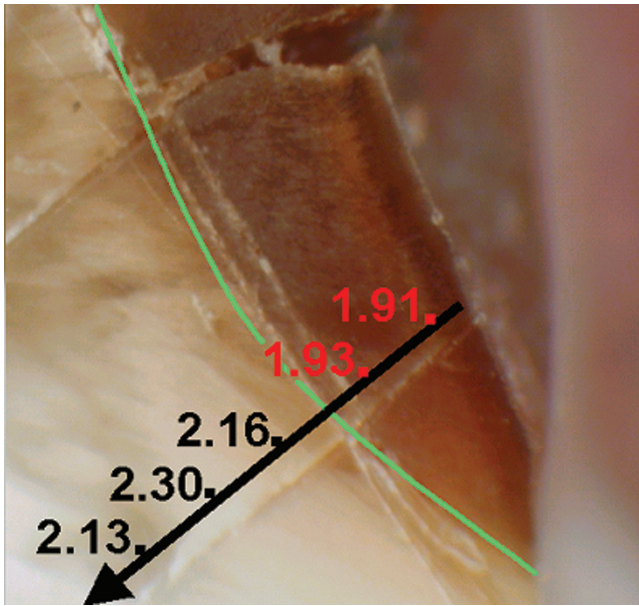


Fig. 4. Showing a selected region from the same tooth as Fig. 3 with a transit marked, along which partial frame lifetimes were taken, across the clinically established decay/stained tissue hardness boundary – marked in green. Lifetime values (shown here in nanoseconds) from within clinically hard but stained and apparently uninvolved dentine were found to be similar, and both reported lifetime values higher than those obtained from decayed softened dentine (cf. Figs 6, 7).

Figure 5 shows a site from close to Fig. 3, panel 1B with a transit marked, along which frame lifetimes were taken across the softened/hard tissue boundary. The clinical interface was defined using a conventional dental probe, establishing an acceptable tissue hardness resection line, suitable for restoration. Lifetime values from within clinically hard but stained and apparently uninvolved dentine were found to be similar to sound dentine values (~ 2.3 ns), but both were higher than values obtained from softened decayed dentine (~ 1.8 – 1.9 ns).

A second sample, imaged at the enamel-dentine junction adjacent to an enamel cavity is shown in Fig. 4. As expected, decayed dentine 488-nm auto-fluorescence demarcated the extent of decay with lateral spreading under relatively sound enamel at the enamel-dentine junction. The micron diameter dentine tubules were imaged, as were the arcs of the Hunter-Schreger bands, evident as incremental growth anomalies in sheets of enamel prisms, close to the enamel-dentine junction, side illuminated by the adjacent auto-fluorescent dentine. A chip in the enamel cavity margin was just visible in the 488-nm mercury-arc-sourced incoherent fluorescence image. This was not well resolved in the PCF images due to light propagation from tissues shelving just beyond the ideal optical focal plane, some scatter and defocus. FLIM mapping confirmed lifetime ranges of 1.4–1.6 ns from this dentine sample just lateral to the main enamel cavitation

site. Clinically, this dentine was undoubtedly involved and softened, undermining the adjacent enamel-dentine junction. Lifetime ranges of 1.75–1.9 ns were noted for the adjacent and presumed sound enamel structure in this specimen. This is unsurprising, as enamel naturally has higher mineral content and lower organic content than sound dentine.

Figure 6 comprises fluorescence, intensity and TPSPC FLIM images of a longitudinally sectioned sound dentine root with a normal overlying cementum surface. The collagen fibres of the adherent periodontal ligament insert into the cement layer, retaining the tooth in life, and may be evidenced by the increased 488-nm excited auto-fluorescence intensity in this region. As the collagen and mineral compositions are similar in dentine and cementum, the overall FLIM mapping shows minimal variation across the field. As this region represents unaffected dentine, the surface level FLIM map serves as a useful control to the images in Fig. 3, demonstrating a close similarity to the FLIM map and distribution data in Fig 3C, panel 3. This point may be of significance in the training of clinical dental practitioners to remove only structurally unsound involved dentine material.

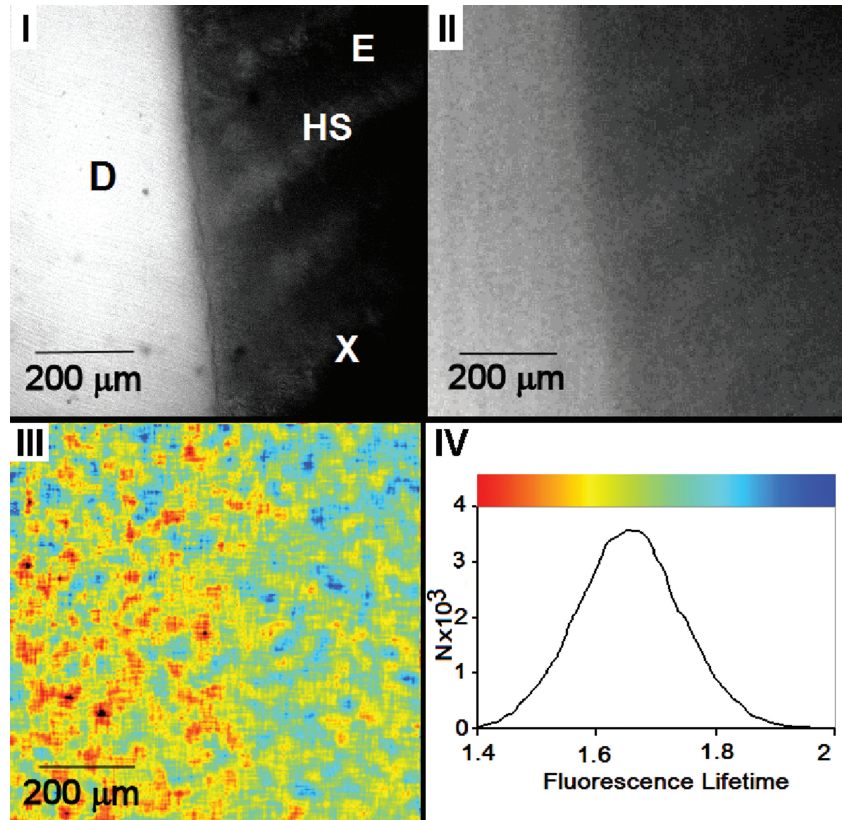
To confirm that optical sampling depth had no influence on the acquired lifetime data (particularly in view of focus difficulties with the PCF images), the FLIM map and fluorescence data were re-acquired at levels 50 and 100 μm beneath the initial surface imaging. As Fig. 6(B) shows, sampling depth through the tissue played no confounding role in the data acquired, despite being derived from mineralized structures perforated by a multitude of light scattering, 1–2 μm diameter, dentinal tubules. Similarly, the cementum region showed no variation with sampling depth and the margin of the sample showed a clean fluorescence cut-off into the adjacent water film at all levels, similar to the dark regions of the tip of the nerve cavity (pulp horn) seen in Fig. 3, panels 1B and 3.

Figure 7 shows another series of whole frame lifetime averages taken for the sites shown, along a transit line scored from an exposed root surface carious lesion (cf. Fig. 3 was coronal) inwards towards the nerve (pulp) chamber. The lifetime data again show a similar significant rise in value on leaving the decayed softened dentine and entering the hard sound material. This lesion shows little hard, uninfected stained dentine along the scored transit, the lesion tending to track along the line of the dentine tubules, curving inferiorly and to the right in this image.

Discussion

This system illuminated by visible blue 488-nm wavelengths generated via PCF adaptation of a Ti:Sapphire source and detecting only in a narrow band pass range 560 ± 25 nm following the protocol of Borisova & Banerjee (Banerjee, 1998; Banerjee & Boyde, 1998; Banerjee *et al.*, 1999, 2003,

Fig. 5. Figure 5 (I) comprises a wide-field autofluorescence image using incoherent mercury arc sourced 488-nm excitation, showing clinically softened dentine (D) at the enamel-dentine junction, just lateral to a shelving enamel cavity margin (X). The micron diameter dentine tubules were visualized, as were the Hunter-Schreger bands (HS), within sound enamel (E), imaged as side-illuminated incremental growth distortions within sheets of enamel prisms, lit by dentine auto-fluorescence, sourced close to the enamel-dentine junction. The enamel cavity margin (X) is visible (bottom right). Within the fluorescence intensity image using the supercontinuum source, some scattering and a nonconfocal, system allowed photons to be recorded from the shelving edge of the enamel cavity margin (x), so it does not appear as a black corner defect in this or the FLIM map lifetime map (III). The corresponding lifetime histogram shows ranges of 1.4–1.55 ns observed for decayed dentine but lifetimes of 1.75–1.9 ns for the sound enamel structure, again showing approximately 40% rise in lifetimes between decayed and sound dental tissues (cf. Fig. 3). The field of view of each image is $630\ \mu\text{m} \times 630\ \mu\text{m}$.



2004; Borisova *et al.*, 2006) tended to ignore the non-metallo-porphyrin spectra that is often quoted. Our data show a detectable and repeatable reduction in fluorescence lifetimes from sound tissue into infected decayed dentine. We attribute this to more sensitive instrumentation. The lifetime assay data in Figs 5 and 7 in particular are in close agreement with Alfano & Yao's figure of 2.3 ± 0.5 ns (530-nm excitation with >560 -nm long pass detection) in the case of sound tissue (Alfano & Yao, 1981). This compares well with previous experiments where 1.8–2.8 ns lifetime range was identified across sound and decayed tissues (Alfano & Yao, 1981; Koenig *et al.*, 1999). Lifetime data with a standard deviation of approximately ± 0.08 ns (Fig. 6) was derived from this experiment, suggesting a real difference in lifetime was detected, as expected for variations in chemistries and physical conditions for a reporting fluorophore across a complex sound tissue–decay lesion interface.

Similarly, Koenig *et al.* reporting on classical long wavelength porphyrin auto-fluorescence with extending lifetime shifts from 10 to ~ 20 ns into decay, also reported two shorter lifetime changes, 0.5–0.3 and 3.2–2.3 ns, respectively, on transit from sound to decayed tissue, (>590 -nm long pass filters) (Koenig *et al.*, 1999). However, their data reported a reduction in the overall contribution of the total fluorescence

by these lifetime signatures due to the dominance of the monomeric porphyrin signatures. In this experiment the long porphyrin lifetimes were not detected and 560 \pm 20 nm bandpass filters were used to further discriminate the enhanced auto-fluorescence-decayed dentine regions. This minimized the porphyrin contribution, thereby investigating an alternative fluorochrome source. Flavins similarly reflect metabolic function and 450-nm excitation can elicit emission at 530 \pm 40 nm, usually with 5-ns lifetimes (Koenig & Schneckenburger, 1994).

Whereas porphyrin molecules including PPIX emit at >650 nm with 10–20 ns lifetimes on excitation at ~ 400 nm, metallo-porphyrins (in particular zinc protoporphyrin) emit at 580 nm and 630 nm with an ~ 2 -ns lifetime (Koenig *et al.*, 1993; Koenig & Schneckenburger, 1994), fitting our findings.

Cariou dentine auto-fluorescence is considered not to be related to lesion mineral content (Alfano & Yao, 1981; Banerjee & Boyde, 1998). However, 430–450 nm dentine auto-fluorescence intensity increases have been reported with 488-nm excitation, after aseptic acidic demineralization (van der Veen & ten Bosch, 1996; Borisova *et al.*, 2006). Subsequent bacterial introduction induced additional 590–650 nm porphyrin fluorescence maxima as expected, further supporting the contention that both tissue dissolution and

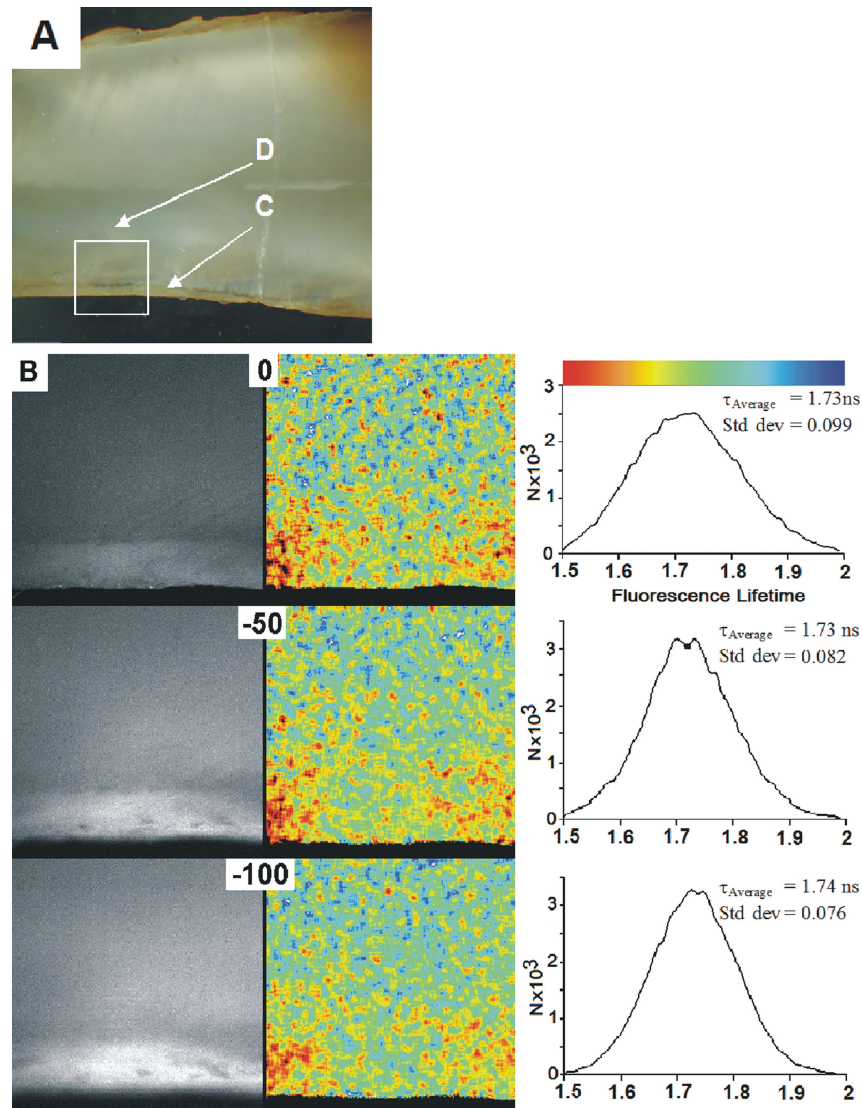


Fig. 6. Part A shows a gross morphology of a longitudinally sectioned sound dentine root with a normal overlying cementum surface (C) in a water film. Figure 6(B) comprises from left to right, fluorescence intensity, corresponding lifetime images and lifetime histograms obtained at increasing depths of 0 μm , -50 μm and -100 μm that is below the surface, across the 630 μm field of view. The overall FLIM mapping shows minimal variation across the field confirming that collagen and mineral compositions are similar in dentine and cementum and that depth of imaging below the surface had no influence on the data measurements (note the data SD were ~ 0.08 ns uniformly across the data acquired in all the experiments). As this region represents nondecayed dentine, the surface level FLIM map serves as a useful control to Figs 3–7. The sample margin showed a clean fluorescence cut-off into the adjacent water film at all levels, similar to the pulp horn in Fig. 3. Inclusion of the sample boundary confirms a negative imaging control. For processing, 7×7 pixel binning was applied.

bacterial colonisation generate independent fluorescence signatures (Borisova *et al.*, 2006).

Individual bacterial species, for example, *Actinomyces odontolyticus*, *Pseudomonas aeruginosa*, *Bacteroides intermedius* can synthesize porphyrins (Koenig *et al.* 1993) and are capable of permeating dentinal tubules (Burnett & Scherp, 1951; Loesche & Syed, 1973) but are minority decay species. The more abundant *Streptococcus mutans* and *Lactobacilli* reportedly

lack significant auto-fluorescence signatures at 488-nm excitation (Koenig *et al.*, 1993; Koenig & Schneckenburger, 1994). There is currently no evidence for exogenous protease auto-fluorescence.

Matsumoto *et al.* reported that although fluorescence intensity, decay times and spectral profiles are constant for all tooth types taken from the same individual and from individuals of the same age, intensity increases and

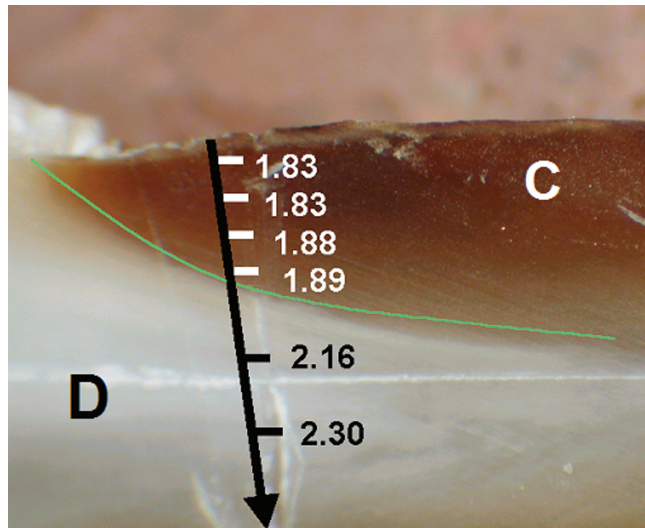


Fig. 7. A partial frame lifetime average data series (in nanoseconds) recorded at regular points along the transit indicated across a sectioned exposed root surface carious lesion (C), towards the dentine (D) encased the nerve (pulp) chamber. A significant lifetime value rise is again noted between the softened decayed (green clinical demarcation line) and hard, sound dentine (cf. Fig. 5). Little hard, uninfected stained dentine is seen in this lesion as the lesion tracked along the line of the dentine tubules, curving apically to the right in this macroscopic image (3-mm-wide field of view).

matched decay time decreases were noted with both ageing and the experimental application of heat (Matsumoto *et al.*, 1999, 2001). This may be a consequence of temperature-dependent physiochemical fluorophore degradation or alteration mechanisms. This further explains why our samples from a range of patients gave dissimilar specific lifetime data for any given tissue, but all showed a uniform trend in behaviour on assessment of sound versus decayed tissue.

Although the zinc protoporphyrin and coenzyme fluorophores are appealing explanations, the similarity to Matsumoto's thermal findings would also support the contention that none of these factors was pertinent in the explanation for this lesion fluorescence and reduced lifetime phenomenon as the mineral and bacteriological contents of the samples were dramatically dissimilar in each experiment. It could be proposed that an inherent dentine matrix component, possibly a collagen, is reporting altered physical conditions, either being modified by bacterial or other physico-chemical mechanisms; measured fluorescence lifetimes shorten due to local quenching variables limiting energy release, such as local ion concentrations, pH, oxygen tension (redox state) and protein binding within biological systems.

Within decayed dentine, a number of environmental regions or phases exist from the surface. First, softened, demineralized and bacterially populated proteolytic zones are found, preceded internally by bacterially infected demineralized zones and

more centrally still, stained but uninfected zones of enhanced mineralization, representing the pulpal defence against decay attack (Banerjee, 1998; Banerjee & Boyde, 1998; Banerjee *et al.*, 1999, 2003, 2004). Undoubtedly, within an infected decay environment, lowered pH, significant redox shifts and molecular constitutions are dramatically altered, all or some of which could quench and thus shorten the detected lifetimes from the auto-fluorescent markers within sound dentine, explaining the life changes reported above. Experimentally obtained scaling between lifetime and a parameter of interest can be used *in vivo* to obtain a map of physiological parameter changes that can then serve as a base for an *in vivo* specific diagnostic or resection control system (Gannot *et al.*, 2004).

Modern thoughts on teaching clinicians to prepare decayed teeth for restoration are biased towards less destructive tooth preparation, the traditional dogma of leaving only fresh dentine being rejected in favour of drilling cessation on detecting hard mineralised tissue, regardless of staining characteristics. The coincidence of the auto-fluorescence boundary and FLIM map interfaces (Figs 5, 7) with the clinically defined soft/hard tissue boundary and not the deeper affected stained tissue fits well with the modern clinical tenets.

Given the relatively narrow range of excitation wavelengths employed, the lack of amplitude flatness of the WLS is not a concern. Furthermore, it is evident that the estimated sub-mW average excitation powers are more than adequate for FLIM imaging. From this, we can assume that a supercontinuum source spanning a wider range of wavelengths (e.g. that reported by Price *et al.* (2003)) could also serve as a more flexible excitation source, even when taking into account the comparable decrease in average power within the same spectrally filtered wavelengths.

Conclusion

We have demonstrated the first application of a WLS source for TCSPC FLIM on human dental samples. Using an existing conventional fs-pulsed Ti:Sapphire laser as the pump for a 30-cm long section of PCF, conventional intensity imaging and TCSPC FLIM of sound and decayed dentine, enamel and cementum were performed at modest excitation power. Sub- μm spatial and sub-ns temporal resolutions were observed using the respective imaging methods. Over a typical 300-s imaging period, no specimen degradation was observed but valuable change in fluorescence lifetime data and thus signature chemical condition or composition changes across the health/decay affected/decay infected interfaces in dentinal disease were obtained by this novel technique.

We also plan to extend the application of a WLS source for FRET/FLIM. The FRET technique utilizes a distance-dependent interaction between the electronic excited states of two dye molecules where excitation energy is nonradiatively transferred from a donor molecule to an acceptor molecule. As the efficiency of the FRET process varies with the inverse

sixth power of the intermolecular separation, this method enables the investigation of a range of biological processes with spatial resolution beyond the limits of conventional optical microscopy. We will therefore apply the WLS source for FRET/FLIM to simultaneously retrieve temporally resolved information from fluorescently labelled samples, with the aforementioned molecular-scale resolution but with a truly wavelength-flexible excitation source. We envisage that the range of wavelengths available from the WLS source will significantly broaden the range of FRET pairs that can currently be imaged using either single-photon or multiphoton excitation.

Further improvements to the laser source will also be investigated. Use of a pulse picker or a diode laser with variable repeat rates would allow us to selectively examine longer lifetime fluorophores to expand the breadth of potential fluorophores examinable in the system, but our intention was to derive a white-light laser source using pre-existing equipment at minimal increased cost, to examine the nonporphyrin auto-fluorescence characteristics of decayed dentine. In recent work a commercially available digital mirror (as used in a digital light projector) has been integrated with a PCF fibre source and a spectrally dispersive optic to give a source whose spectrum can be rapidly altered to match a wide range of fluorophores (McConnell *et al.*, 2006). By adopting this approach, we hope to perform TCSPC FLIM of a wider range of biological specimens in the near future. Furthermore, from previous experiments using a WLS source for confocal laser scanning fluorescence microscopy (McConnell, 2004), four-dimensional TCSPC FLIM is possible and we will investigate this in due course.

The results on the dental samples demonstrate that it is possible to distinguish between decayed dentine, stained but hard dentine and healthy dentine. This indicates that time-resolved methods may be suitable for helping in the preparation of teeth for restoration. Potentially, this could lead to the removal of less healthy tissue and thus improved treatments resulting in a lower failure rate for restorations and thus a higher quality of life for the patient.

Acknowledgements

The authors wish to acknowledge funding from the Royal Society of Edinburgh and Research Councils UK (GMcC), DoH Clinician Scientist Training Fellowship Number BS/DHCS/03/G121/55 (RC) and Cancer Research UK.

References

- Alfano, R.R. & Yao, S.S. (1981) Human teeth with and without dental caries studied by visible luminescent spectroscopy. *J. Dent. Res.* **60**, 120–122.
- Ameer-Beg, S.M., Barber, P.R., Hodgkiss, R.J., Locke, R.J., Newman, R.G., Tozer, G.M., Vojnovic, B. & Wilson, J. (2002) Application of multiphoton

- steady-state and lifetime imaging to mapping of tumour vascular architecture *in vivo*. *Proc. SPIE* **4620**, 85–95.
- Ameer-Beg, S.M., Edme, N., Peter, M., Barber, P.R., Ng, T.C. & Vojnovic, B. (2003) Imaging protein-protein interactions by multiphoton FLIM. *Proc. SPIE* **5139**, 180–189.
- Anilkumar, N., Parsons, M. & Monk, R. (2003) Interaction of fascin and protein kinase C alpha: a novel intersection in cell adhesion and motility. *EMBO J.* **22**, 5390–5402.
- Banerjee, A. & Boyde, A. (1998) Auto-fluorescence and mineral content of carious dentine: scanning optical and backscattered electron microscopic studies. *Caries Res.* **32**, 219–226.
- Banerjee, A. (1998) *Applications of scanning microscopy in the assessment of Dentine Caries and methods of its removal*. PhD Thesis, University of London.
- Banerjee, A., Sherriff, M., Kidd, E.A.M. & Watson, T.F. (1999) A confocal microscopic study relating the auto-fluorescence of carious dentine to its microhardness. *Br. Dent. J.* **187**, 206–210.
- Banerjee, A., Kidd, E.A.M. & Watson, T.F. (2003) In vitro validation of carious dentin removed using different excavation criteria. *Am. J. Dent.* **16**, 228–230.
- Banerjee, A., Gilmour, A., Kidd, E.A.M. & Watson, T.F. (2004) Relationship between *S. mutans* and the auto-fluorescence of carious dentin. *Am. J. Dent.* **17**, 233–236.
- Barber, P.R., Ameer-Beg, S.M., Gilbey, J., Edens, R.J., Ezike, I. & Vojnovic, B. (2005) Global and pixel kinetic data analysis for FRET detection by multi-photon time-domain FLIM. *Proc. SPIE* **5700**, 171–181.
- Becker, W., Benndorf, K., Bergmann, A., Biskup, C., König, K., Tirplapur, U. & Zimmer, T. (2001) FRET measurements by TCSPC laser scanning microscopy. *Proc. SPIE* **4431**, 414–419.
- Becker, W., Bergmann, A., Hink, M.A., König, K., Benndorf, K. & Biskup, C. (2004) Fluorescence lifetime imaging by time-correlated single-photon counting. *Microsc. Res. Tech.* **63**, 58–66.
- Borisova, E., Uzunov, T. & Avramov, L. (2006) Laser-induced auto-fluorescence study of caries model in vitro. *Lasers Med. Sci.* **21**, 34–41.
- Buchalla, W. (2005) Comparative fluorescence spectroscopy shows differences in noncavitated enamel lesions. *Caries Res.* **39**, 150–156.
- Burnett, G.W. & Scherp, H.W. (1951) Bacteriologic studies of the advancing dentinal lesion. *J. Dent. Res.* **30**, 766–770.
- Carlsson, K. & Liljeborg, A. (1989) A confocal laser microscope scanner for recording of optical serial sections. *J. Microsc.* **153**, 171–180.
- de Grauw, J.C. & Gerritsen, H.C. (2001) Multiple time-gate module for fluorescence lifetime imaging. *Appl. Spectrosc.* **55**, 670–678.
- Elson, D.S., Siegel, J., Webb, S.E.D., Lévêquefort, S., Parsons-Karavassilis, D., Cole, M.J., French, P.M.W., Davis, D.M., *et al.* (2002) Wide-field fluorescence lifetime imaging with optical sectioning and spectral resolution applied to biological samples. *J. Mod. Opt.* **49**, 985–995.
- Fedotov, A.B., Zheltikov, A.M., Lvanov, A.A., Alfimov, M.V., Chorvat, D., Beloglazov, V.I., Mel'nikov, L.A., Skibina, N.B., *et al.* (2000) Supercontinuum-generating holey fibers as new broadband sources for spectroscopic applications. *Laser Phys.* **10**, 723–726.
- Foreman, P.C. (1980) The excitation and emission spectra of fluorescent components of human dentine. *Arch. Oral Biol.* **25**, 641–647.
- Gadella, T.W. & Jovin, T.M. (1995) Oligomerization of epidermal growth factor receptors on A431 cells studied by time-resolved fluorescence imaging microscopy: a stereochemical model for tyrosine kinase receptor activation. *J. Cell Biol.* **129**, 1543–1558.
- Gannot, I., Ron, I., Hekmat, F., Chernomordik, V. & Gandjbakhche, A. (2004) Functional optical detection based on pH dependent fluorescence lifetime. *Lasers Surg. Med.* **35**, 342–348.

- Haak, R. & Wicht, M.J. (2004) Caries detection and quantification with DIAGNOdent: prospects for occlusal and root caries? *Int. J. Comput. Dent.* **7**, 347–358.
- Koenig, K. & Schneckenburger, H. (1994) Laser induced autofluorescence for medical diagnosis. *J. Fluoresc.* **4**, 17–40.
- Koenig, K., Hibst, R., Meyer, H., Flemming, G. & Schneckenburger, H. (1993) Laser induced auto-fluorescence of carious regions of human teeth and caries-involved bacteria. *SPIE*. **2080**, 170–180.
- Koenig, K., Boehme, S., Leclerc, N. & Ahuja, R. (1998) Time-gated auto-fluorescence microscopy of motile green microalga in an optical trap. *Cell Mol. Biol.* **44**, 763–770.
- Koenig, K., Schneckenburger, H. & Hibst, R. (1999) Time-gated in vivo auto-fluorescence imaging of dental caries. *Cell. Mol. Biol.* **45**, 233–241.
- Kurihara, E., Koseki, T., Gohara, K., Nishihara, T., Ansai, T. & Takehara, T. (2004) Detection of subgingival calculus and dentine caries by laser fluorescence. *J. Periodontal Res.* **39**, 59–65.
- Kwak, E.S., Kang, T.J. & Vanden Bout, D.A. (2001) Fluorescence lifetime imaging with near-field scanning optical microscopy. *Anal. Chem.* **15**, 3257–3262.
- Lamb, D.C., Muller, B.K. & Brauchle, C. (2005) Enhancing the sensitivity of fluorescence correlation spectroscopy by using time-correlated single photon counting. *Curr. Pharm. Biotechnol.* **6**, 405–414.
- Loesche, W.J. & Syed, S.A. (1973) The predominant cultivable flora of carious plaque and carious dentine. *Caries Res.* **7**, 201–216.
- Marriott, G., Clegg, R.M., Arndt-Jovin, D. & Jovin, T.M. (1991) Time resolved imaging microscopy. Phosphorescence and delayed fluorescence imaging. *Biophys. J.* **60**, 1374–1387.
- Matsumoto, H., Kitamura, S. & Araki, T. (1999) Auto-fluorescence in human dentine in relation to age, tooth type and temperature measured by nanosecond time-resolved fluorescence microscopy. *Arch. Oral Biol.* **44**, 309–318.
- Matsumoto, H., Kitamura, S. & Araki, T. (2001) Applications of fluorescence microscopy to studies of dental hard tissue. *Front. Med. Biol. Eng.* **10**, 269–284.
- Maus, M., Rousseau, E., Cotlet, M., Schweitzer, G., Hofkens, J., van der Auweraer, M., De Schryver, F.C. & Krueger, A. (2001) New picosecond laser system for easy tunability over the whole ultraviolet/visible/near infrared wavelength range based on flexible harmonic generation and optical parametric oscillation. *Rev. Sci. Instrum.* **72**, 36–40.
- McConnell, G. (2004) Confocal laser scanning fluorescence microscopy with a visible continuum source. *Opt. Express* **12**, 2844–2852.
- McConnell, G., Poland, S. & Girkin, J.M. (2006) Fast wavelength multiplexing of a white-light supercontinuum using a digital micromirror device for improved three-dimensional fluorescence microscopy. *Rev. Sci. Instrum.* **77**, 13702–13708.
- Mendes, F.M., Hissadomi, M. & Imparato, J.C. (2004) Effects of drying time and the presence of plaque on the in vitro performance of laser fluorescence in occlusal caries of primary teeth. *Caries Res.* **38**, 104–108.
- Mujat, C., van der Veen, M.H., Ruben, J.L., ten Bosch, J.J. & Dogariu, A. (2003) Optical path-length spectroscopy of incipient caries lesions in relation to quantitative light-induced fluorescence and lesion characteristics. *Appl. Opt.* **42**, 2979–2986.
- Mujat, C., van der Veen, M.H., Ruben, J.L., Dogariu, A. & ten Bosch, J.J. (2004) The influence of drying on quantitative laser fluorescence and optical path lengths in incipient natural caries lesions. *Caries Res.* **38**, 484–492.
- Ng, T., Parsons, M., Hughes, W.E., Monypenny, J., Zicha, D., Gautreau, A., Arpin, M., Gschmeissner, S., et al (2001) Ezrin is a downstream effector of trafficking PKC-integrin complexes involved in the control of cell motility. *EMBO J.* **20**, 2723–2741.
- O'Connor, D.V. & Phillips, D. (1984) *Time Correlated Single Photon Counting*. Academic Press, London.
- Odetti, P.R., Borgoglio, A. & Rolandi, R. (1992) Age-related increase of collagen fluorescence in human subcutaneous tissue. *Metabolism* **41**, 655–658.
- Price, J.H.V., Monro, T.M., Furusawa, K., Belardi, W., Baggett, J.C., Coyle, S.J., Netti, C., Baumberg, J.J., et al. (2003) UV generation in a pure-silica holey fibre. *App. Phys. B* **77**, 291–298.
- Schneckenburger, H. & Koenig, K. (1992) Fluorescence decay kinetics and imaging of NAD(P)H and flavins as metabolic indicators. *Opt. Eng.* **31**, 1447–1451.
- Schomacker, K.T., Frisoli, J.K., Compton, C.C., Flotte, T.J., Richter, J.M., Deutsch, T.F. & Nishioka, N.S. (1992) Ultraviolet laser-induced fluorescence of colonic tissue: basic biology and diagnostic potential. *Lasers Surg. Med.* **12**, 63–78.
- Schonle, A., Glatz, M. & Hell, S.W. (2000) Four-dimensional multiphoton microscopy with time-correlated single-photon counting. *App. Opt.* **39**, 6306–6311.
- Stortelder, A., Buijs, J.B., Bulthuis, J., Gooijer, C. & van der Zwan, G. (2004) Fast-gated intensified charge-coupled device camera to record time-resolved fluorescence spectra of tryptophan. *Appl. Spectrosc.* **58**, 705–710.
- Taubinsky, I.M., Alexandrov, M.T., Kos'ma, S.Y. & Chernyi, V.V. (2000) Prospects for applying fluorescence spectroscopy to diagnose the hard tissues of a tooth. *Crit. Rev. Biomed. Eng.* **28**, 137–144.
- van der Veen, M.H. & ten Bosch, J.J. (1996) The influence of mineral loss on the auto-fluorescence behaviour of in vitro-demineralised dentine. *Caries Res.* **30**, 93–99.
- van der Veen, M.H. & de Josselin de Jong, E. (2000) Application of quantitative light-induced fluorescence for assessing early caries lesions. *Monogr. Oral Sci.* **17**, 144–162.
- Vroom, J.M., de Grauw, K.J., Gerritsen, H.C., Bradshaw, D.J., Marsh, P.D., Watson, G.K., Birmingham, J.J. & Allison, C. (1999) Depth penetration and detection of pH gradients in biofilms by two-photon excitation microscopy. *Appl. Environ. Microbiol.* **65**, 3502–3511.
- Webb, W.W., Lévêque-Fort, S., Elson, D.S., Siegel, J., Watson, T.F., Lever, M.J., Booth, M., Juskaitis, R., et al. (2002) Wavelength-resolved 3-dimensional fluorescence lifetime imaging. *J. Fluores.* **12**, 279–283.